IRAQI Academic Scientific Journals

Samarra Journal of Pure and Applied Science

SJPAS

www.sjpas.com

p ISSN: 2663-7405
e ISSN: 2789-6838

Optical formulation and searchlight styling Fabry- Perot Interferometer

Suran Dunun Yaseen*

Department of Information Technology, Khabat Technical Institute, Erbil Polytechnic University, Erbil, Iraq

https://doi.org/10.54153/sjpas.2022.v4i1.357

Article Information

Received: 10/01/2022

Accepted: 20/02/2022

Keywords:

Fabry-Perot Interferometer, ultrasonic waves, style, Reflector, interferometer transport

Corresponding Author

Email: suran.yaseen@epu.edu.iq

Mobile: 07504638017

Abstract

The Fabry-Perot Interferometer (FPI) reflector has an optical definition and style that are used to evaluate ultrasound. By adjusting the division of the deepening of the FPI classification, the ultrasound adjusts the optical table of the column. The difference in predicted light caused by a unit change in the depression thickness is what defines the photosensitivity. Performing an optical design on a Fabry-Perot interferometer to replicate the interferometer transport (IT_v) task of a Gaussian beam. The proliferation of the Gaussian bar stage into the Fabry-Perot interferometer to help translate the replicated IT_v form. This study is used as a planning tool to make the FPI review easier this is achieved by using column sweep, mirror reflection, and depression scattering, which all contribute to the strong optical influence. An FPI evaluation is concluded with a high degree of optical influence and weight linearity. Putting extremely different elements together.

Introduction

The traditional strategy for ultrasonic detection is to use piezoelectric Trans-ducers. The limitations of piezoelectric transducers are acoustic impedance errors and uneven repetitive responses upon exposure to natural tissue and water. Despite the fact that the piezoelectric polymer material polyvinylidene difluoride (PVDF) overcomes these problems, its effectiveness is negligible. High frequency directivity (10 to hundreds of MHz) is required, another constraint develops, requiring a spot measurement that is substantially shorter than the audible wave's wavelength, lowering piezoelectric viewfinder's sensitivity does [1].

The major advantage of optical sensors over piezoelectric sensors is that they can reach higher efficiency with fewer component sizes, especially for high-frequency ultrasound. Optical sensors also have the advantage of not being impacted by electromagnetic fields piezoelectric sensors, for example, have high impedances. You don't need to run a large number of wires If you're putting together an optical sensor cluster, you'll need one for each array Interferometry is one sort of ultrasonic optical inspection technology. One such device is the Fabry-Perot Interferometer (FPI), which detects ultrasonic waves by creating optical phase modulation caused by incident sound pressure waves. Another optical technique for detecting ultrasonic vibrations is fibre Bragg gratings (FBG). The sensors performance of the Fabry-Perot interferometer is being enhanced, especially in the field of photoacoustic imaging. The ability to detect lower pressure amplitude waves is one reason for improved FPI sensor performance [2].

Another motivation is to improve pressure linearity so that a larger range of pressure amplitudes can be detected. To improve the detection sensitivity of photoacoustic images, the specular reflectance increased. The light beam probing the FPI sensors will begin within the FPI, diffracting resulting in a loss of sensitivity. As a result, determining the appropriate parameters for achieving high detection sensitivity is critical. It's also critical to consider how to increase pressure linearity in applications such as ultrasonic metrology and classic ultrasonic detection methods, Optical sensors and their detection techniques are also included. A specific sort of Fabry-Perot interferometer in its current configuration sensor for photoacoustic imaging is introduced. The Fabry-Perot interferometer's analytical model for non-divergent beams.

Ultrasonic and photoacoustic wave detection methods.

Ultrasonic technology has been around for a long time. The piezoelectric effect is employed in detectors and happens in crystal-like resources or piezoelectric ceramics [1]. The piezoelectricity is an optically translucent electromechanical event that happens in crystal-like resources or piezoelectric porcelains. When a piezoelectric material is subjected to mechanical strain, the alternating voltage from across material varies. When the practical voltage through a material fluctuates, mechanical contraction or expansion occurs, producing ultrasonic vibrations. On the crystal, the dipole moment induces charge dispersion, which causes the voltage to change. A change in charge distribution occurs as a result of the impact pressure wave, and this causes a shift in voltage all across material. The impedance incongruity amid the ground and the piezoelectric sensor affects the detection capability of incident ultrasonic waves. Reflections are caused by incongruity amid the average and the indicator. The density of piezoelectric materials and the speed at which sound waves propagate through them determine their characteristic acoustic impedance.

Table1: Property of Piezoelectric Substance with Distinct Textures

Element	encyclopedic effects speed (longitudinal) (m/s)	Width ρ (g/cm^3)	Distinctive phonic resistance z^0 (10^6 kgm^{-2} s^{-1})
Quartz (x-cut)	5700	2.65	15.3
Lead zirconate titanate (PZT5A)	4350	7.75	33.7
Lead Metaniobate	3330	6.0	20.5
Water	1	1480	1.48
longitudinal waves	1.9	2800	5.32

Table (1) lists the properties of a variety of piezoelectric resources and the possessions of numerous mankind matters. Despite its high sensitivity, PZT's acoustic impedance is not comparable to that of water or human tissues. The piezoelectric polymer material polyvinylidene diflouride (PVDF) has an impedance acoustic closer to water and several other human tissues because the amplitude of the acoustic reflection is low, resulting in a uniform frequency response and causing the detector to work at particular frequencies. The lower resonance's frequency is reduced. PVDF has a poor sensitivity, which is a drawback [3].

The transducer constant D, which is recognized like the practical power to the voltage, is used to determine a transducer's sympathy.

$$D = \frac{eA}{t} \quad (1)$$

Where (e) represents the charge of electron, (A) represents the superficial zone, and (t) represents the transducer depth [1]. The sensitivity of a transducer is measured by the transducer constant S. A lesser indicator zone A will result in a lower compassion. This is due to the fact that as the element size lowers, the overall potential of the transducer surface area drops. Smaller components are required when the detector must be omnidirectional, and the spatial resolution of the sound wave front to be detected is improved.

Interferometer Theory

A Fabry-Perot Interferometer is made up two reedy partly shinning and transferring looking glasses. The distance between the two mirrors of a planar Fabry-Perot Interferometer (FPI) is l_0, and the middle amid the two mirrors has a refractive catalogue that differs from the surrounding medium's refractive index ns, as shown in Figure 1. The Fabry-Perot Interferometer [4] divides the amplitude of electromagnetic waves to create an interferometer. The illumination incident mirror, which has a fullness replication constant of r_1, partially reflects the incident ray. The mirrors reflect and transmit each incident of the transmitted beam into the cavity. The beam makes a complete round trip when an electric field with amplitude coefficient r_1' is incident on the interior surface of mirror 1 after traveling twice the mirror separation $2l_0$. As a result, the electric field is interfered with by the mirrored scopes $Er_{,2}$, $Er_{,3}$, $Er_{,4}$ that are sent hole $E_{r,1}$.

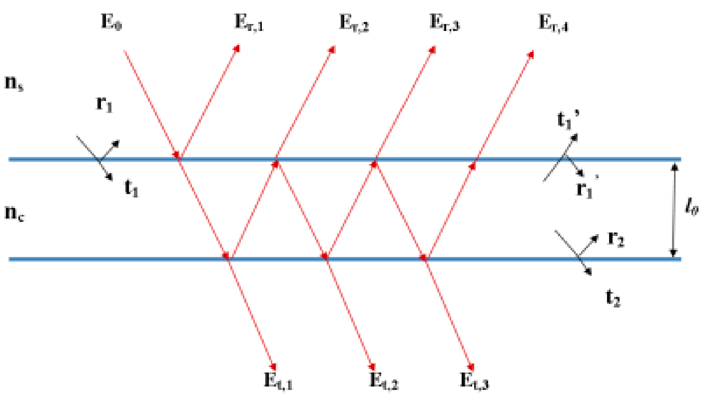

Figure 1: Fabry Perot Interferometer with r_1 and r_1' largeness looking glass likeness constants for mirror 1 and r_2 amplitude mirror reflection coefficients for looking glass 2. The conduction largeness constants for mirrors 1 and 2 are t_1 and t_2, correspondingly, with conduction t1' from within the hole at mirror 1.

The electric field E that strikes the FPI is defined via its stage and early largeness E_0. A non-diverging plane wave electric field is assumed in the following study. When the entire electric fields sent from the hole at image 1 are added together, interference with the incident mirror's reflected field occurs. The electrostatic current in the cavity changes phase, causing destructive interference with the electronic scope returned from the first image. In terms of phase, the Interferometry Transfer Function ITv_φ is the result of this. If there is no reflection mode, the transmission mode ITv supplements the reflection mode ITv_φ

$$E_1 = t_1^2\, r_2 e^{-i(k2l-2\pi vt)} E_0$$

$$E_2 = t_1^2\, r_2^2\, r_1'\, e^{-i(k4l-2\pi\nu t)} E_0$$
$$E_3 = t_1^2\, r_2^3\, r_1'^2\, e^{-i(k6l-2\pi\nu t)} E_0 \quad (2)$$
$$\dots\dots\dots\dots\dots$$
$$\dots\dots\dots\dots\dots$$
$$E_m = t_1^2\, r_2^m\, r_1'^{(m-1)}\, e^{-i(k2ml-2\pi\nu t)} E_0$$

r_1' and t_1' are the largeness image and conduction coefficients of looking glass 1 within the hole, respectively, while t_1 is the incoming mirror's amplitude transmission coefficient. Mirror 2 has r_2 and t_2 as Coefficients of amplitude reflection and transmission, respectively. A complete round trip distance of 2m1 is propagated, where m is the rotund journey amount and value of two is owing to the beam crossing twice the cavity spacing l to back looking glass 1. Eq.2 shows the total number of electronic scopes which have made m amount of rotund journey with the first mirror's imitated electric field.

$$E_{total} = r_1 E_0 e^{(kz-2\pi\nu t)} + \sum t_1 t_1'\, r_1'^{(m-1)}\, r_2^m E_0 e^{\,i(k2ml-2\pi\nu t)} \quad (3)$$

where r_1' and t_1' are the largeness image and conduction coefficients of looking glass 1 within the hole, respectively, and t_1 is the incoming mirror's amplitude transmission coefficient. Looking glass 2's largeness image and conduction constants are r_2 and t_2. Eq. 3 indicates the total amount of electric forces that have travelled (m) number of times around the round with the replicated electric field of the initial mirror.

Fabry Perot Interferometers

For optical ultrasonic detection, Perot Frafry interferometers (FPI) are utilized [5], [6],[7],[8]. These are sensed between 100 and 500 kHz at the landfill of the visual character there is absorption in front of the audio source. The FPI's ultrasonic detecting mechanism is as follows. As sound waves collide with the FPI sensor, the cavity's thickness varies. The optical phase of the beam changes as the cavity thickness changes [9], leading in a variation in the replicated or communicated well-lit of FPI [10],[11],[12] the highest gradient of the Interferometer Transferal Role (ITν) . Figure 2 depicts the process for identifying sound waves. As a pressure wave reaches the FPI sensors, the cavity width varies. As a result, the incident light utilized to search for FPI has a phase change, causing reflected light to shift as well. Photo acoustic imaging has a lot of potential with FPI sensors [13].

The photo acoustic frequency is usually in the rule with a smallest visible burden of 0.2 kPa [14], with a minimum detectable the hollow has a thickness of tens of microns, reaching from 10 to 80 microns, and is often used in FPI sensors. This is a fraction of the wavelength of an acoustic wave. The visual FPI device has a unchanging rate reply of 39 MHz to a 3 dB and a detector element that is several dozens of microns in size. The FPI sensors wideband nature allows it to be monitored at a low frequency of several hundred KHz, compared to excessively resonant conventional piezoelectric detectors.

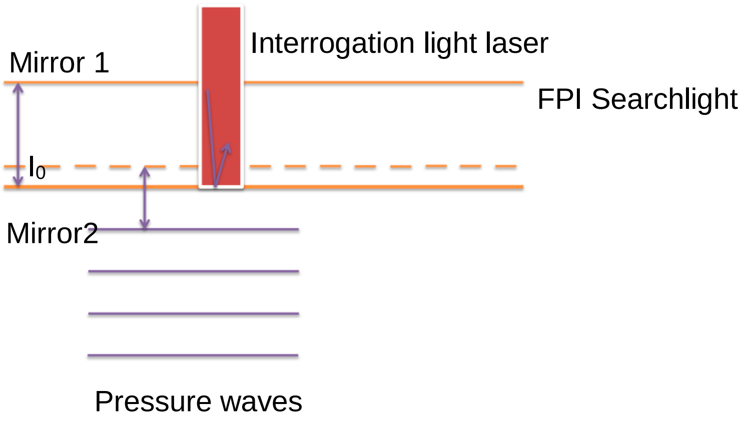

Figure 2: Apparatus of identifying audial waves, because the strain contracts the width of the hollow space modifications which adjust the strength of the pondered light

Optical Inspection sensitivity

The highest slope of the Interferometer Transferal Role (ITν's) peak reflectance or transmittance is used to polarize the FPI sensors. A basic Airy model is used to generate the definitions of ITν and optical sensitivity. The influence of ray deviation and non-uniformity can lead the ITν to leave from the perfect unconcerned role in a high-definition FPI structure with a specular reflectance greater than 90% [13].

Light sensitivity, also known as light phase compassion, is recognized like the variation in replicated light when the phase of the light changes slightly. The non-divergent beam's light's round-trip phase in the cavity is given as,

$$\varphi = \frac{4\pi n l}{\lambda} \qquad (4)$$

(l) Is the distance between the cavities, n denotes the refractive catalogue, and λ denotes the wavelength. This point is linked to the $ITν_{\phi}$ point via the Light R role, like seen below:

$$R = \frac{FSin\,(\frac{\varphi}{2})^2}{1 + FSin(\frac{\varphi}{2})^2} \qquad (5)$$

Where F is the finesse coefficient. As a result, the highest alteration in mirrored light dY happens at the all-out of Eq.5's copied with admiration to stage. This is known as S_0 visual sympathy, and it is recognized like,

$$S_0 = \frac{dY}{d\varphi} \qquad (6)$$

Where dY/dφ is Plagiaristic of the period $ITν_{\varphi}$

(7) $$S_A = \frac{d\varphi}{dP} = \frac{4\pi n l}{\lambda E} \qquad (5)$$

Definition of sensitivity for an FPI Inspection

The produce of the visual sympathy S_0 recognized in Eq.6 with the aural sympathy description S_A in Eq.7 recognizes the total sympathy S. The sympathy is consequently stated like:

$$S = \frac{dY}{dP} = \frac{dY}{d\varphi}\frac{d\varphi}{dP} \quad (8)$$

$$S = \frac{dY}{d\varphi}\frac{4\pi n}{\lambda}\frac{l}{E} \quad (9)$$

The cavity thickness of the speaker bandwidth must meet certain acoustic sensitivity standards. The spacer material that makes up the FPI cavity also has mechanical and optical qualities. As a result, an FPI sensor with higher optical sensitivity is required to boost sensitivity. Increased specular reflection can be used to create FPI sensors with increased optical sensitivity. The radius of the beam employed, on the other hand, is on the instruction of tens of microns, and the range of non-diffraction in it is equal to or less than the distance it goes back and forth in the cavity[15]. As a result, the beam in the cavity will diverge, causing the ITν to deviate from the perfect Airy function. This is related to the beam's divergence pitch. As a result, in order to mimic the propagation of Gaussian beams in FPI, a model must be built. This will help in the selection of the appropriate ray range, specular reflectance, and other optical characteristics for high optical sensitivity Guo's job as a model to detect pressure waves. On a thin cavity low thickness ITν, a burden movement with a 1 mm waist is used. This is a fairly decent solution that allows for pressure sensitivity and linearity. The plane beam incident on the FPI sensor can be used to approximate these characteristic [16].

Design and manufacture of FPI Inspection

FPI inspection and manufacturing scheme

The optical searchlight of the FPI is made up of two mirror coatings separated by a Parylene C insulating level shown in Figure 3, the FPI searchlight constructed on an optically clear organic glass substrate.

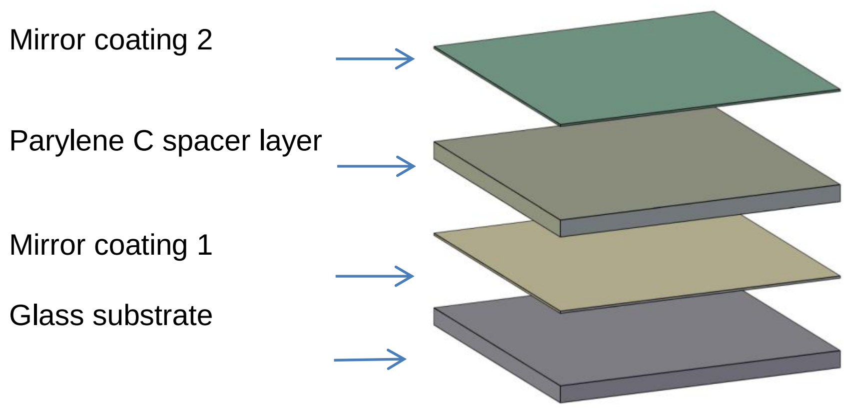

Figure 3: The FPI searchlight, which is made of optically clear methacrylate, has a unique design.

The substrate is implanted to avert scrounging interfering generated by the Fresnel image coefficient, which is shaped when the refractive catalogue of the organic glass and the surrounding medium differs [9]. Quarter-wave stacks of high and low refractive index materials make up dielectric mirrors. A vacuum sputtering technique deposits the primary mirror (coating 1) directly on the substrate. On top of the initial coating, the insert cover amid the mirror is placed. the everyday thickness of the outlet created is within the tens of microns range. Because the sound waves are within the sub-millimetre to 1 millimetre region, this could attain a wider acoustic bandwidth. The spacer layer is created from the polymer Parylene C, that's within the sort of particles and is animated to provide a gas before being vacuum-deposited on the sensor employing a chemical vapour deposition process [17],[18],[19]. Then, on ParyleneC, apply the second mirror coating (coating 2). Finally, a coating of ParyleneC film is applied to the sensor to stop water intrusion and abrasion shown in Figure3.

Creating optimized designs Interferometer searchlight from Fabry- Perot

The development and testing of a model that simulates ITvs for an FPI lit through a Gaussian beam. A considerate of the form of the ITvs was offered, mainly for diverging rays, as well as how the form of the ITv is affected via a piece angle. The findings are necessary for comprehending the project and optimization of the FPI device described in this paper. The metrics that quantify the performance of the FPI sensor are presented. Like the ray radii and looking glass reflectivities are modified, the metric's value changes, requiring the selection of optical parameters for an optimized FPI sensor. Various examples of FPI sensors are considered to place the plan of FPI devices into framework. The pressure linearity that may be obtained while maintaining great optical sensitivity was also demonstrated [20].

Influence of shaft of light deviation and looking glass reflection on the ITv$_\lambda$

When lighting FPIs with various looking glass reflectivity, the effect of increasing the beam radius on the ITv$_\lambda$s is shown in the current subsection. ITv$_\lambda$s for an inferometer with a hollow density 50 m looking glass reflectivity's of 0.90, 0.95, and 0.98 percent are shown in Figure 4.

The ITv$_\lambda$s for a 10 μm incident photons range are shown in Figure 4(a). The reflectivity peaks become narrower as the mirror reflectance increases, while the asymmetry increases. Due to the early round trips via the scope in the cavity contribute more to the timbre than for lesser mirror reflectivities, the asymmetry grows with mirror reflectivity.

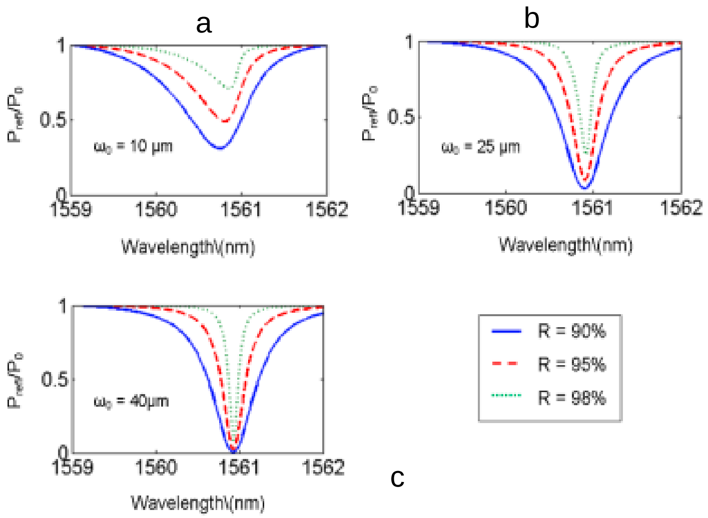

Figure 4: ITv$_\lambda$s for a FPI with hole width

With bigger mirror reflectivity’s, the Gouy phase's impact on the shape of the mirror is reduced. $IT\nu_\lambda$ becomes more pronounced. As the reflectance minimum increases, visibility decreases. As the ray range approaches 25 m, the eyesight for R=90 percent improves, as the reflectivity of the mirror increases, it decreases. As the mirror reflectivity grows, the reflectivity top contracts. When the FPI is encountered with a 40-meter beam range, the pattern is similar. The following is a summary of the overall trend among $IT\nu_\lambda$s:

• The reflectance peak sharpens as the reflectivity of the mirror increases for all beam radii; however, it becomes asymmetric for small beam radii.

• Visibility decreases as looking glass reflectivity rises for wholly ray ranges, nonetheless the decrease is smaller for greater ray ranges. This is due to the fact that greater beam radii are closer to the greater Rayleigh series z_0, the beam is non-diverging.

Cumulative the looking glass reflectivity’s is thought to improve optical sensitivity. Diffraction effects, on the other hand, would cause $IT\nu_\lambda$s to stray from a non-deviating ray. This would bound the visual sympathy for differences in mirror reflectivity’s and, in some situations, reduce it. As a result, this chapter explains how to select the best ray range and looking glass reflectivity’s for the best visual compassion. The ability to characterize the fineness and visibility variations as a function of ray range and looking glass reflectivity is critical in determining the requisite visual limits. The fineness and visibility variations with beam are presented in the next sub-section mirror reflectivity and radius.

Relationship of Airy Role with Segment and sensivity definition

The segment expressed in Eq.10 is related to hole spacing l and refractive catalogue n_c, as shown.

$$\varphi = \frac{4\pi n_c \mathrm{L}}{\lambda} \qquad (10)$$

The wavelength λ is inversely proportionally to the phase. Consequently the stage Period Interferometer Transferal Role ($IT\nu\varphi$) is the overturn of the wavelength $IT\nu\lambda$. This is significant like these contracts via wavelength Interferometer Transferal Role ($IT\nu\lambda$s). As a result, the phase shift between each round trip is constant Changes in $IT\nu$ as a task of segment restrictions. Variation of the $IT\nu$ with respect to different phase parameter as seen in Eq.10, phase has an inverse relationship with wavelength. As a result, shorter wavelengths correspond to lower phase values, while longer wavelengths correspond to higher phase values, as seen in Figure 5, which displays the inverse relationship between phase and wavelength.

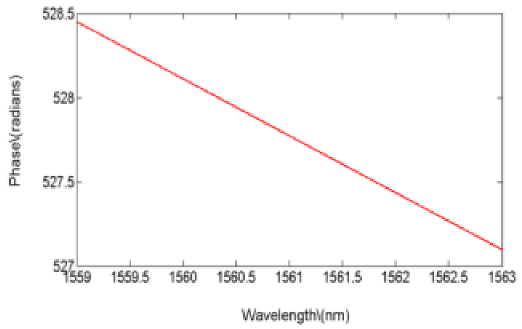

Figure 5: The phase of a wave corresponds to the length of the wave.

Consequently the copied of the ITν$_L$ in wavelength planetary would have the all-out sympathy at extended wavelengths like described in Figure 6.

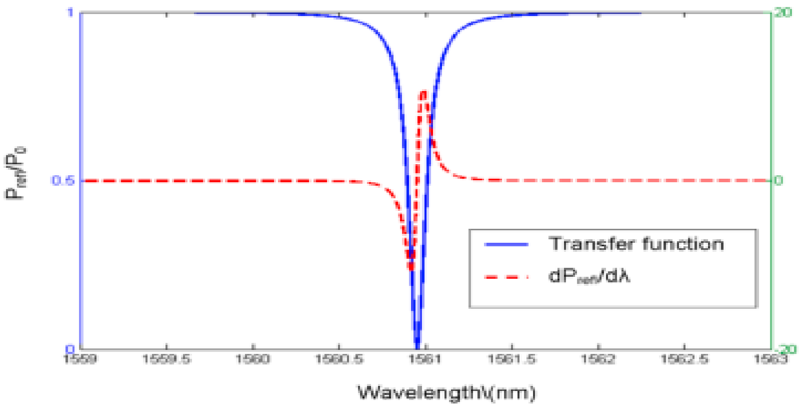

Figure 6: Chart of ITν$_\lambda$ in contradiction of wavelength λ, and dY/dλ in contradiction of wavelength λ.

The Airy role and derived of the normalised reflected energy Y with phase (dY/dφ), as well as the equivalent value for dY/dλ on dY/dφ, are shown in Figure 7. The all-out of Derivative of the wavelength ITν$_\lambda$ (dY/dλ) corresponds to the least of dY/dφ, as can be observed. The Airy role characterization for non-diverging beams is used in this investigation. The optical beams accustomed probe the FPI sensors are divergent Gaussian rays specified by the TE$_{00}$ style, can impact the FPI's involved subtlety.

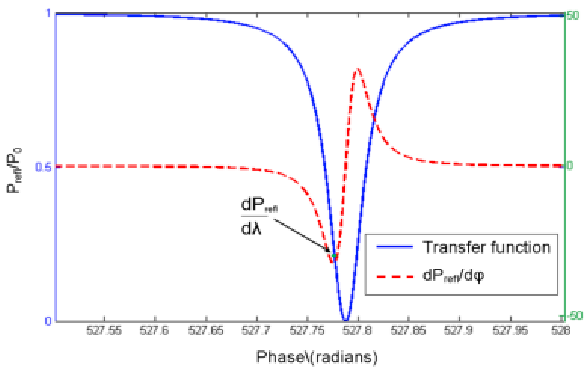

Figure 7: for 0.95 mirror reflectivity's, a diagram of the Airy role and dY/dφ as a result of period and the determined of dY/dλ is shown.

Optical sensitivity expressions

The Airy function is used to express the explicit statement of optical sensitivity. The derivative of the Airy function, which fluctuates with phase, defines the optical phase sensitivity:

$$\frac{dY}{d\emptyset} = \frac{\vartheta \sin\left(\frac{\emptyset}{2}\right)\cos\left(\frac{\emptyset}{2}\right)}{1+\vartheta \sin^2\left(\frac{\emptyset}{2}\right)} - \frac{\vartheta \sin^3\left(\frac{\emptyset}{2}\right)\cos\left(\frac{\emptyset}{2}\right)}{\left(1+\vartheta \sin^2\left(\frac{\emptyset}{2}\right)\right)^2} \tag{11}$$

Equation 11 is an explicit expression based on the Airy function for optical phase sensitivity. The expression's highest and minimum values agree to the points on the ITϑ_φ where the all-out light variation happens for dφ. Conversely, because the whole depth is controlled in ultrasound sensing, the optical sensitivity can be described as,

$$\frac{dY}{d\emptyset} = \left[\frac{\vartheta \sin\left(\frac{\emptyset}{2}\right)\cos\left(\frac{\emptyset}{2}\right)}{1+\vartheta sin^2\left(\frac{\emptyset}{2}\right)} - \frac{\vartheta sin^3\left(\frac{\emptyset}{2}\right)\cos\left(\frac{\emptyset}{2}\right)}{(1+\vartheta sin^2(\frac{\emptyset}{2}))^2}\right]\frac{4\pi n}{\lambda} \tag{12}$$

The wavelength ITν$_\lambda$ derivative, that is utilized to determine the best wavelength to interview the FPI device, is recognized like,

$$\frac{dY}{d\emptyset} = \left[\frac{\vartheta \sin\left(\frac{\emptyset}{2}\right)\cos\left(\frac{\emptyset}{2}\right)}{1+\vartheta sin^2\left(\frac{\emptyset}{2}\right)} - \frac{\vartheta sin^3\left(\frac{\emptyset}{2}\right)\cos\left(\frac{\emptyset}{2}\right)}{(1+\vartheta sin^2(\frac{\emptyset}{2}))^2}\right]\frac{4\pi nl}{\lambda^2} \tag{13}$$

Equations 12 and 13 indicate that the optical sensitivity reduce for resonance modes corresponding to longer wavelengths. Because of the dielectric mirrors' structure, the wavelengths sensors is probed in photo acoustic are in the telecoms bandwidth. Biasing at optical wavelengths would result in an FPI with a poor fineness.

Conclusions

The many ultrasonic detection systems have been detailed, as well as some of their drawbacks. Some of these restrictions can be overcome with optical sensors based on Fabry-Perot interferometry. Photo acoustic imaging is one of FPI's applications. It discusses the FPI sensor's photo acoustic effect and current structure for PA picturing, and it can be used for medical photo acoustic picturing. The Fabry-Perot interferometer can handle clinical and biological imaging scenarios that need great sensitivity and a large acoustic bandwidth. The goal of this is to improve the plan of devices for a diversity of uses in the scope of medicinal ultrasound by modelling the optical properties of FPI. This is accomplished through increasing optical sensitivity to detect ultrasonic waves from deeper tissue layers, and picturing the aural wave front with improved three-dimensional resolve and sympathy via utilizing larger ray ranges.

This study could aid in the widespread adoption of Fabry-Perot interferometers in a diversity of uses. The Fabry Perot is used in vibration discovery and strain measuring in industrial machinery and aircraft construction to determine the magnitude of vibrations, in addition to ultrasonic detection. The Fabry-Perot interferometer has been used to measure temperature, as well as humidity. The hole is modified via a boiler action of the whole insertion coating when recording the temperature, which variations the stage of the ray in the hole. The Fabry-Perot optical interferometer sensor is also utilized in chemical analysis applications to change the refractive index of liquid material between cavities to determine the chemical composition of the liquid material. As a result, the knowledge of the parameters that determine detection sensitivity gained in this study can be applied to the creation of better Fabry-Perot detectors.

References

1.H.Kuttruff, Acoustics: An Introduction (Taylor & Francis, 2004).

2. P. C. Beard and T. N. Mills, "Extrinsic optical fibre ultrasound sensor using a thin polymer film as a low finesse Fabry-Perot interferometer", *Appl. Opt.*, vol. 35, no. 4, pp. 663-675, 1996.

3. P. C. Beard and T. N. Mills, "A miniature optical fibre ultrasonic hydrophone using a Fabry-Perot polymer film interferometer", *Electron. Lett.*, vol. 33, no. 9, pp. 801-803, 1997.

4. F. L. Pedrotti and L. M. Pedrotti, Introduction to Optics (2rd Edition) (Pearson Education Limited, 2006), p. Chapter 27.

5. B. Lee, "Review of the present status of optical fiber sensors," Opt. Fiber Technol. 9, 57–79 (2003).

6. Q. Sun, N. Chen, Y. Ding, Z. Chen, and T. Wang, "Optical Fiber Extrinsic Fabry-Perot Interferometer Sensors for Ultrasound Detection," in SPIE Proceedings, X. Li, Q. Luo, V. Ntziachristos, and Y. Yasuno, eds. (2009), Vol. 7634, pp. 763410–1 – 763410–7.

7. E. Hansis, T. Cubel, J.-H. Choi, J. R. Guest, and G. Raithel, "Simple pressure-tuned Fabry–Pérot interferometer," Rev. Sci. Instrum. 76, 033105–1 – 033105–3 (2005).

8. S. Liu, Y. Wang, C. Liao, G. Wang, Z. Li, Q. Wang, J. Zhou, K. Yang, X. Zhong, J. Zhao, and J. Tang, "High-sensitivity strain sensor based on in-fiber improved FabryPerot interferometer.," Opt. Lett. 39, 2121–2124 (2014).

9. E. Zhang, J. Laufer, and P. Beard, "Backward-mode multiwavelength photoacoustic scanner using a planar Fabry-Perot polymer film ultrasound sensor for high-resolution three-dimensional imaging of biological tissues.," Appl. Opt. 47, 561–577 (2008).

10. C. Sheaff and S. Ashkenazi, "Polyimide-etalon all-optical ultrasound transducer for high frequency applications," in Proceedings of SPIE, A. A. Oraevsky and L. V. Wang, eds. (2014), Vol. 8943, pp. 8943M–1 – 8943M–8.

11. K.-S. Kim, Y. Mizuno, and K. Nakamura, "Fiber-optic ultrasonic hydrophone using short Fabry-Perot cavity with multilayer reflectors deposited on small stub.," Ultrasonics 54, 1047–1051 (2014).

12. S. Rajagopal, B. Zeqiri, and P. Gélat, "Calibration of miniature medical ultrasonic hydrophones for frequencies in the range 100 to 500 kHz using an ultrasonically absorbing waveguide.," IEEE Trans. Ultrason. Ferroelectr. Freq. Control 61, 765–768 (2014).

13. B. J. Slagmolen, M. B. Gray, K. G. Baigent, and D. E. McClelland, "Phase-sensitive reflection technique for characterization of a fabry-perot interferometer.," Appl. Opt. 39, 3638–3643 (2000).

14. B. T. Cox and P. C. Beard, "The frequency-dependent directivity of a planar fabryperot polymer film ultrasound sensor.," IEEE Trans. Ultrason. Ferroelectr. Freq. Control 54, 394–404 (2007).

15. D. Guo, R. Lin, and W. Wang, "Gaussian-optics-based optical modeling and characterization of a Fabry-Perot microcavity for sensing applications," JOSA A 22, 1577–1588 (2005).

16. P. R. Wilkinson and J. R. Pratt, "Analytical model for low finesse, external cavity, fiber Fabry – Perot interferometers including multiple reflections and angular misalignment," Appl. Opt. 50, 4671–4680 (2011).

17. P. Morris, "A Fabry-Perot fibre-optic hydrophone for the characterisation of ultrasound fields," University of London (2008).

18. O. I. Szentesi and E. A. Noga, "Parylene C Films for Optical Waveguides," Appl. Opt. 13, 2458–2459 (1974).

19. H. T. Kim, T. Koo, and C. Park, "Parylene-C thin films deposited on polymer substrates using a modified chemical vapor condensation method," Korean J. Chem. Eng. 27, 748–751 (2010).

20. Yaseen, S. D. (2021). Fabry-Perot interferometer and mode matching. *Samarra Journal of Pure and Applied Science*, *3*(4), 160-168.

IRAQI Academic Scientific Journals

Samarra Journal of Pure and Applied Science

SJPAS

مجلة سامراء للعلوم الصرفة والتطبيقية

www.sjpas.com

p ISSN: 2663-7405
e ISSN: 2789-6838

صياغة بصرية وتصميم كشاف مقياس التداخل فابري- بيروت

سوران ذوالنون ياسين

قسم تكنلوجيا المعلومات، معهد خبات التقني، جامعة اربيل التقنية - العراق

https://doi.org/10.54153/sjpas.2022.v4i1.357

معلومات البحث:

تأريخ الاستلام: 2022/01/10

تأريخ القبـــول: 2022/02/20

الكلمات المفتاحية

مقياس التداخل Fabry-Perot ، الموجات فوق الصوتية ، النمط ، العاكس ، نقل مقياس التداخل.

معلومات المؤلف

الايميل suran.yaseen@epu.edu.iq

الموبايل: 07504638017

الخلاصة:

يحتوي عاكس مقياس التداخل فابري بيروت (FPI) على تعريف وأسلوب بصري يتم استخدامه لتقييم الموجات فوق الصوتية. من خلال ضبط تقسيم تعميق تصنيف يقوم الموجات فوق الصوتية بضبط الجدول البصري للعمود. الاختلاف في الضوء المتوقع الناجم عن تغيير الوحدة في سمك المنخفض هو ما يحدد الحساسية للضوء. إجراء تصميم بصري على مقياس تداخل فابري-بيروت لتكرارنقل مقياس التداخل (ITv) لشعاع غاوسي. تكاثر مرحلة شريط غاوسي في مقياس التداخل فابري بيروت للمساعدة في ترجمة النسخ المتماثل ITv المكرر.تُستخدم هذه الدراسة كأداة تخطيط لتسهيل مراجعة FPI ، ويتم تحقيق ذلك باستخدام مسح العمود وانعكاس المرآة وتشتت الانخفاض ، والتي تساهم جميعها في التأثير البصري القوي. يتم الانتهاء من تقييم FPI بدرجة عالية من التأثير البصري